Signatures of the chiral two-pion exchange electromagnetic currents in the ^{2}H and ^{3}He photodisintegration reactions

D. Rozpędzik,[1] J. Golak,[1] S. Kölling,[2,3] E. Epelbaum,[4] R. Skibiński,[1] H. Witała,[1] and H. Krebs[4]

[1]*M. Smoluchowski Institute of Physics, Jagiellonian University, PL-30059 Kraków, Poland*

[2]*Forschungszentrum Jülich, Institut für Kernphysik (IKP-3) and Jülich Center for Hadron Physics, D-52425 Jülich, Germany*

[3]*Helmholtz-Institut für Strahlen und Kernphysik (Theorie) and Bethe Center for Theoretical Physics, Universität Bonn, D-53115 Bonn, Germany*

[4]*Institut für Theoretische Physik II, Ruhr-Universität Bochum, D-44780 Bochum, Germany*

(Received 26 March 2011; published 28 June 2011)

The recently derived long-range two-pion exchange (TPE) contributions to the nuclear current operator that appear at next-to-leading order (NLO) of the chiral expansion are used to describe electromagnetic processes. We study their role in the photodisintegration of ^{2}H and ^{3}He and compare our predictions with the experimental data. The bound and scattering states are calculated using five different parametrizations of the chiral next-to-next-to-leading order (N^{2}LO) nucleon-nucleon (NN) potential, which allows us to estimate the theoretical uncertainty at a given order in the chiral expansion. For some observables the results are very close to the predictions based on the AV18 NN potential and the current operator (partly) consistent with this force. In most cases, the addition of long-range TPE currents improved the description of the experimental data.

DOI: 10.1103/PhysRevC.83.064004 PACS number(s): 25.20.−x, 21.30.−x, 21.45.−v, 24.70.+s

I. INTRODUCTION

Chiral effective field theory (ChEFT) provides a systematic and model-independent framework to analyze hadron structure and dynamics in harmony with the spontaneously broken approximate chiral symmetry of QCD. This approach is a powerful tool for the derivation of the nuclear forces. Exchange vector and axial currents in nuclei have also been studied in the framework of ChEFT. Since the pioneering work of Park *et al.* [1], heavy-baryon chiral perturbation theory has been applied to derive exchange axial and vector currents for small values of the photon momentum. These calculations have been carried out in time-ordered perturbation theory. The resulting exchange vector currents have been, in particular, applied to analyze radiative neutron-proton capture within a hybrid approach [2].

ChEFT has also been used to study the electromagnetic properties of the deuteron [3,4] and ^{3}He [5,6]. One of the fundamental processes observed for the deuteron is the photodisintegration reaction. It has been a subject of intense experimental and theoretical research for several decades (see Refs. [7,8]). Also photodisintegration of ^{3}He has been studied experimentally and theoretically for a long time [9–11]. Photodisintegration observables provide a good tool for studying the contributions from meson exchange currents (MEC) to the nuclear current operator. This is because the charge density operator, which often dominates low-energy electrodisintegration and is mostly given by the single nucleon current, does not play any role in this reaction. An ongoing interest in low-energy photodisintegration reactions, especially in view of planned experiments, provides a strong motivation to apply the framework of chiral effective field theory. This approach relies on the approximate spontaneously broken chiral symmetry of QCD. It allows for a systematic derivation of the nuclear Hamiltonian and the corresponding electromagnetic current operator from the underlying effective Lagrangian for pions and nucleons via the chiral expansion (i.e., a simultaneous expansion in soft momenta of external particles and about the chiral limit). For more details on the application of ChEFT to nuclear forces and currents the reader is referred to recent review articles [12,13] and references therein.

In the two- and three-nucleon systems, the leading contributions to the exchange current originate from one-pion exchanges which are well known. The $2N$ current operator at the leading loop order in the chiral expansion has been worked out by Pastore *et al.* [14,15] based on time-ordered perturbation theory. Independently, the two-pion exchange $2N$ current operator has been derived in Ref. [16] using the method of unitary transformation. The resulting current operator is consistent with the corresponding chiral two-nucleon potential [12] obtained within the same scheme. In the present work, for the first time we explore the effects of the leading two-pion exchange $2N$ operator [16] in the photodisintegration reactions of ^{2}H and ^{3}He. We, however, emphasize that the presented calculations are not yet complete. In particular, the corresponding expressions for the one-pion exchange at next-to-leading order (NLO) and short-range contributions to the current operator within the method of unitary transformation are not yet available. Our main goal in the present work is to explore the sensitivity of various observables in the deuteron and ^{3}He photodisintegration to the two-pion exchange current rather than to provide a complete description of these reactions within the ChEFT framework.

Our manuscript is organized as follows. In Sec. II the formalism which we use to describe selected $2N$ electromagnetic reactions is presented. The results for the photodisintegration of the ^{2}H are discussed and compared with the experimental data in Sec. III. The extension to the 3N system is briefly described in Sec. IV and the results obtained for the photodisintegration of ^{3}He are presented in Sec. V. Finally, Sec. VI contains the summary and conclusions.

II. FORMALISM

The general form of the nuclear matrix element for electromagnetic disintegration reactions in the $2N$ system is represented by

$$N^\mu \equiv \left\langle \Psi^{2N}_{\rm scatt} \middle| J^\mu(\vec{Q}) \middle| \Psi^{2N}_{\rm bound} \right\rangle, \tag{2.1}$$

where the proton-neutron scattering state $|\Psi^{2N}_{\rm scatt}\rangle$ and the deuteron bound state $|\Psi^{2N}_{\rm bound}\rangle$ are obtained using the nucleon-nucleon (NN) potential. The current operator $J^\mu(\vec{Q})$ acts between the internal initial and final $2N$ states. We employ the solution of the Lippmann-Schwinger equation $t = V_{2N} + tG_0V_{2N}$ to express N^μ as

$$N^\mu = \langle \vec{p}_0|(1 + tG_0)\, J^\mu(\vec{Q}) \big| \Psi^{2N}_{\rm bound} \rangle, \tag{2.2}$$

where G_0 is the free $2N$ propagator, t is the NN t matrix and $|\vec{p}_0\rangle$ is the eigenstate of the relative proton-neutron momentum. Since all observables can be computed from N^μ, the description of the electromagnetic reactions requires the knowledge of the consistent potential and electromagnetic current. The NN potential based on ChEFT is currently available up to next-to-next-to-next-to-leading order in the chiral expansion [12,13]. As already pointed out, in this paper we focus on the long-range two-pion exchange (TPE) contributions to the current operator, which appear at NLO. However, to avoid the theoretical error from using the less accurate NLO NN potential, all calculations are made using the next-to-next-to-leading order ($\rm N^2LO$) potential. At this order, the NN potential V_{2N} is built from the one-pion exchange (OPE), $V_{1\pi}$, and TPE, $V_{2\pi}$, contributions as well as various contact interactions (cont) [12]

$$V_{2N} = V_{1\pi} + V_{2\pi} + V_{\rm cont}. \tag{2.3}$$

The effective current operator J^μ for the $2N$ system is a sum of the single-nucleon operators $J^\mu(i)$, $i = 1, 2$ and two-nucleon operators of different type [$J^\mu(1, 2)$]

$$J^\mu = J^\mu(1) + J^\mu(2) + J^\mu(1, 2), \tag{2.4}$$

where

$$J^\mu(1, 2) = J^\mu_{1\pi}(1, 2) + J^\mu_{2\pi}(1, 2) + J^\mu_{\rm cont}(1, 2). \tag{2.5}$$

The expressions for the single-nucleon and the leading OPE currents $J^\mu_{1\pi}(1, 2)$ are well established (see e.g., Ref. [17]). The results for the leading TPE contributions used in the present work are available in Refs. [14,16]. We emphasize that the resulting TPE current is parameter free. The expressions for the OPE and contact currents at the leading loop level have been recently worked out within time-ordered perturbation theory [15]. Work on the derivation of these contributions using the method of unitary transformation is still in progress.

The $2N$ four-current operator $J^\mu(1, 2) \equiv [J^0(1, 2), \vec{J}(1, 2)]$ can be decomposed according to its isospin and spin-momentum structure and quite generally written in the form [16,18]

$$J^0(1, 2) = \sum_{\eta=1}^{5} \sum_{\beta=1}^{8} f^{\beta S}_\eta(\vec{q}_1, \vec{q}_2) T_\eta O^S_\beta, \tag{2.6}$$

$$\vec{J}(1, 2) = \sum_{\eta=1}^{5} \sum_{\beta=1}^{24} f^{\beta}_\eta(\vec{q}_1, \vec{q}_2) T_\eta \vec{O}_\beta, \tag{2.7}$$

where $\vec{q}_i \equiv \vec{p}\,'_i - \vec{p}_i$ is the momentum transferred to nucleon i, T_η is the $2N$ isospin operator, O^S_β and $\vec{O}_\beta$ are the (momentum-dependent) spin operators in the $2N$ space, $f^{\beta S}_\eta$ and f^β_η are scalar functions. The explicit form of the scalar functions and the operator basis for O^S_β and $\vec{O}_\beta$ can be found in Ref. [16].

In this paper, we concentrate on a treatment of the long-range TPE contributions to the $2N$ current operator derived in Ref. [16]. The expressions for the functions $f^{\beta S}_\eta(\vec{q}_1, \vec{q}_2)$ and $f^\beta_\eta(\vec{q}_1, \vec{q}_2)$ entering the TPE current and charge density operators in Eqs. (2.6) and (2.7) are rather complicated and contain the standard loop functions and the three-point functions in a form suitable for numerical calculations [16]. Due to their isospin structure, not all combinations of Eqs. (2.6) and (2.7) contribute to the photodisintegration of the deuteron. The nonvanishing contributions emerge from

$$\begin{aligned} \vec{J}_{2\pi}(1, 2) = &\sum_{\beta=3}^{10} f^\beta_2(\vec{q}_1, \vec{q}_2)\, (\vec{\tau}_1 - \vec{\tau}_2)_3\, \vec{O}_\beta \\ &+ f^2_3(\vec{q}_1, \vec{q}_2)\, (\vec{\tau}_1 \times \vec{\tau}_2)_3\, \vec{O}_2, \end{aligned} \tag{2.8}$$

where $(\cdots)_3$ denotes the third Cartesian component of the vector. We work in momentum space and apply the standard partial wave decomposition of the $2N$ potential (see, e.g., Ref. [19] for more details). Our calculations are performed using a complete set of $2N$ states

$$|p\alpha\rangle \equiv |p(ls)jm_j\rangle|tm_t\rangle, \tag{2.9}$$

where p is the magnitude of the relative momentum, l, s, j, and m_j are the orbital angular momentum, spin, total angular momentum, and its projection on the quantization axis $\hat{z}$, respectively. The isospin quantum numbers of the two-nucleon system are denoted by t and m_t.

The TPE current operator needs to be expressed in the same partial wave basis. To this end, we first prepare all spin and isospin matrix elements using MATHEMATICA and then calculate the resulting four-fold angular integrals

$$\begin{aligned} \langle p'\alpha'|\vec{J}_{2\pi}(1, 2)|p\alpha\rangle &= \langle p'(l's')j'm_{j'}; t'm_{t'}|\vec{J}_{\eta\beta}|p(ls)jm_j; tm_t\rangle \\ &= \int d\hat{p}'\, d\hat{p} \sum_{m_l, m'_l} C(l's'j'; m_{l'}, m_{j'} - m_{l'}, m_{j'})\, Y^*_{l'm_{l'}}(\hat{p}')\, C(lsj; m_l, m_j - m_l, m_j)\, Y_{lm_l}(\hat{p}) \\ &\quad \times f^\beta_\eta(\vec{q}_1, \vec{q}_2)\, \langle t'm_{t'}|T_\eta|tm_t\rangle\, \langle s'\, m_{j'} - m_{l'}|\vec{O}_\beta|s\, m_j - m_l\rangle, \end{aligned} \tag{2.10}$$

numerically. Here, $C(lsj; m_l, m_j - m_l, m_j)$ denote the Clebsch-Gordon coefficient and $Y_{lm_l}(\hat{p})$ are the spherical harmonics. Such an approach has been described in Ref. [20]. To calculate the four-fold integrals in Eq. (2.10) for the whole grids of p and p' points and all nonvanishing (α, α', m_j) combinations we used the parallel supercomputer IBM Blue Gene/P of the Jülich Supercomputing Center (JSC).

III. RESULTS FOR PHOTODISINTEGRATION OF THE DEUTERON

We now discuss the results for the deuteron photodisintegration process for the unpolarized cross section and selected polarization observables. The results for the differential cross section, the photon analyzing power, and outgoing proton polarization at the photon laboratory energies of $E_\gamma = 10$, 30, and 60 MeV are shown in Fig. 1. The bands reflect the uncertainty due to the variation of the two cutoff parameters Λ and $\tilde{\Lambda}$ that appear in the chiral potential. While the first cutoff parameter Λ appears in the regulator function for the Lippmann-Schwinger equation, the second parameter $\tilde{\Lambda}$ enters the spectral function regularization (SFR) and denotes the ultraviolet cutoff value in the mass spectrum of the TPE potential. Following Ref. [12], the cutoff values are varied between 450 and 600 MeV for Λ and between 500 and 700 MeV for $\tilde{\Lambda}$. It is important to emphasize that the resulting bands probably overestimate the theoretical uncertainty that can be expected in a complete calculation at this order in the chiral expansion. This is because we have not yet included the corresponding short-range contributions to the nuclear current, which are expected to absorb a large part of the cutoff dependence. Thus, the interpretation of the bandwidth in the obtained results in terms of the theoretical uncertainty should be taken with care. The different bands shown in Fig. 1 describe the contributions from the different parts of the $2N$ current: single-nucleon current (light band), OPE contribution (hatched band), and the long-range TPE contributions (dark band). As a reference, we also show the results based on the phenomenological AV18 potential [21] and the corresponding current model [22,23]. Notice that the results obtained solely from the single nucleon currents and by adding the OPE contributions do not describe the data well and differ significantly from the reference AV18 predictions. An explicit inclusion of the TPE contributions yields an improved description of the experimental data, which turns out to be in agreement with the AV18 predictions. The OPE predictions give the cross section and photon analyzing power values lower than the AV18 results. The bands including TPE currents are broad, however, for $E_\gamma = 30$ and 60 MeV they give a reasonable description of the experimental data. In the case of photon analyzing powers, the best agreement between all models is obtained at lowest energy. For energies $E_\gamma = 30$ and 60 MeV, calculations including the TPE currents yield even better agreement with the experimental data than the AV18 results. It remains to be seen whether this conclusion will still hold after including the short-range and the subleading OPE currents. It is further important to emphasize that the single nucleon current alone is insufficient to describe the data for this observable. Thus, it is necessary to include higher-order electromagnetic currents. In the case of the outgoing proton polarization, we observe a smaller sensitivity to the TPE currents and a good agreement between the traditional framework (AV18) and chiral results at all energies considered. The larger sensitivity to the details of the exchange currents is only observed at forward and backward outgoing proton angles.

We have also calculated the deuteron tensor analyzing powers as a function of the proton emission angle for two E_γ energy bins. Here, we focus on a comparison of our calculations with the recent experimental tensor analyzing powers T_{2q} for low energies from Ref. [25] and do not show the results for vector analyzing power iT_{11} as there exist no experimental data for this observable. To be able to compare the theoretical calculations with the data from Ref. [25], our predictions for the exclusive observables have been integrated over the relevant intervals of the initial photon energy and angular regions. In Fig. 2 the results for the angular distribution at the bin energies of $E_\gamma = 25$–45 MeV and $E_\gamma = 45$–70 MeV together with the experimental data are presented. For all deuteron tensor analyzing powers one observes a rather good agreement between the AV18 potential prediction, chiral results, and experimental data. The effects of the TPE contributions turn out to be very small. Also, no broadening of the bands with increasing photon energy is observed. All this suggests that the deuteron tensor analyzing powers are driven by the long-range parts of the current and are not sensitive to the short-range contributions. We further emphasize some disagreement with the data for T_{21} at forward angles. In the future, it would be interesting to see whether these conclusions are affected by the inclusion of the subleading OPE terms in the current operator.

Finally, we have also calculated the total cross section. This observable was extensively studied in many publications using various theoretical approaches (see, e.g., Ref. [7]). In Fig. 3, the total cross section for $E_\gamma \approx 2$–80 MeV is presented. The experimental data are taken from Refs. [7,8]. In the left panel, we see the results for the single nucleon and OPE current. For this particular case the width of the prediction band is negligible. The theoretical predictions agree rather well with the experimental data. The right panel in this figure shows that the effects of the TPE currents are clearly visible, especially at higher photon energies. We also notice that the bandwidth increases significantly once the TPE contributions are included.

To conclude, we observe that for all considered observables the $2N$ current operator plays an important role and a restriction to the single nucleon current operator leads to a strong disagreement with the data. The inclusion of the leading OPE current is absolutely necessary to achieve a decent description of the experimental data. The effects of the TPE current are clearly visible in the differential cross section and some polarization observables such as Σ^1 and P_y. One also observes a rather good agreement between the results based on ChEFT and the AV18 potential combined with the corresponding current operators.

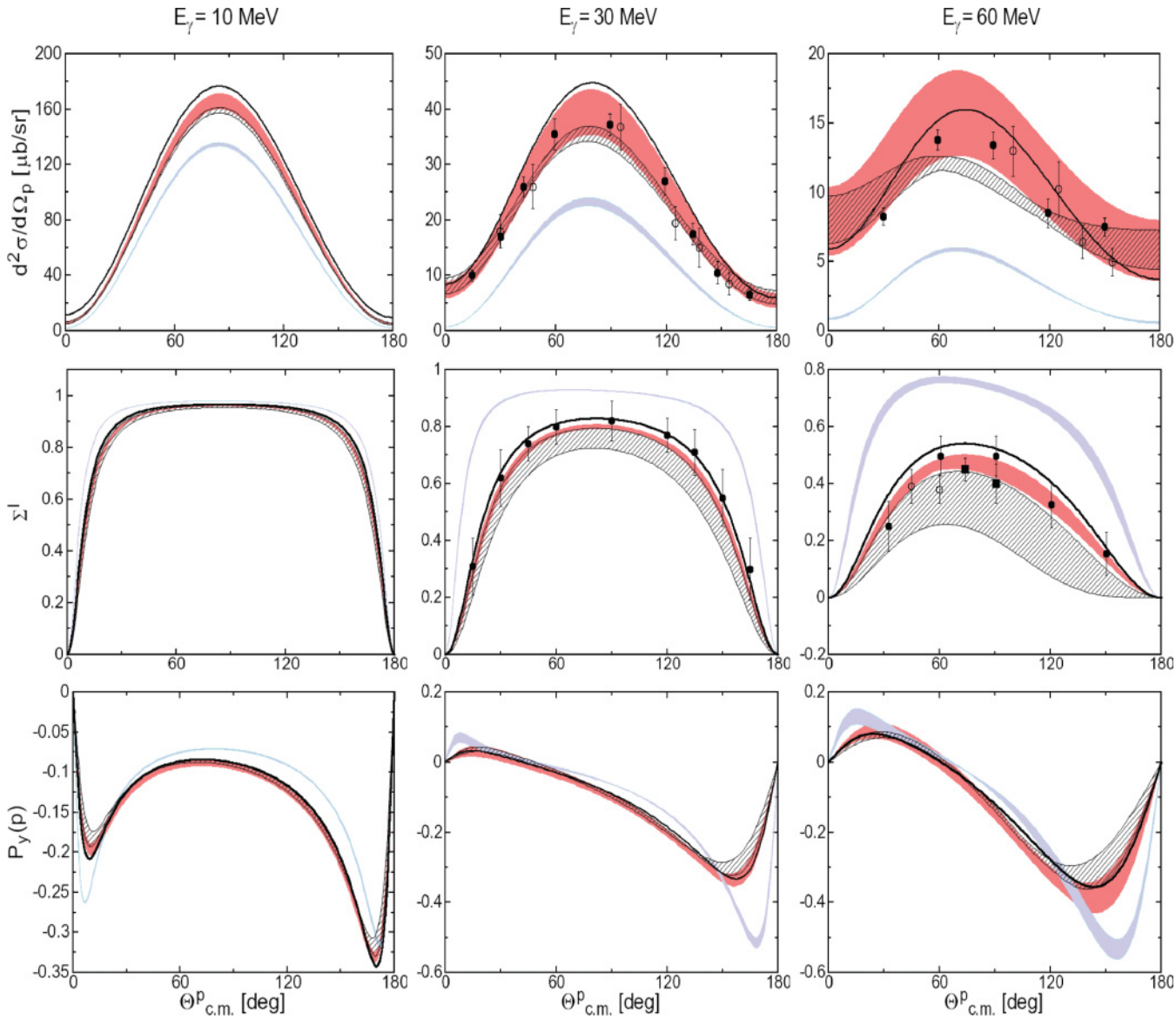

FIG. 1. (Color online) The results for the unpolarized cross section, the photon analyzing power, and outgoing proton polarization in the deuteron photodisintegration process at the photon laboratory energies of $E_\gamma = 10, 30, 60$ MeV, displayed as functions of the proton emission angle. The solid black line refers to the standard calculation based on the AV18 potential, the light (blue) band covers results obtained with the single-nucleon current only, the hatched band represents the predictions based on the single-nucleon and OPE parts and the dark (pink) band includes, in addition, the contributions of the TPE current. The experimental data are from Ying *et al.* [24].

IV. TWO-PION EXCHANGE CURRENTS IN THE 3*N* SYSTEM

For $3N$ reactions, we use the framework and its numerical implementation described in detail in Ref, [11]. In this work, we will only briefly introduce the key points focusing mainly on the current operator in the $3N$ system. The starting point is exactly the same as for the $2N$ reaction. We consider the general matrix element of the current operator between the $3N$ bound state, $|\Psi^{3N}_{\text{bound}}\rangle$, and scattering state $|\Psi^{3N}_{\text{scatt}}\rangle$ for the $3N$ system

$$N^\mu \equiv \langle \Psi^{3N}_{\text{scatt}} | J^\mu(\vec{Q}) | \Psi^{3N}_{\text{bound}} \rangle. \tag{4.1}$$

The $3N$ bound state $|\Psi^{3N}_{\text{bound}}\rangle$ is obtained in the standard way from the appropriate Faddeev equation [26]. The current operator $J^\mu(\vec{Q})$ acts effectively between the internal initial and final $3N$ states. These internal states are conventionally expressed in the momentum space in terms of two Jacobi momenta, $\vec{p}$ and $\vec{q}$ [19]. The momentum $\vec{p}$ describes a relative motion within a $2N$ subsystem (here we choose the subsystem consisting of nucleons 2 and 3). The momentum $\vec{q}$ describes the motion of the spectator nucleon (here nucleon 1) with respect to that $2N$ subsystem

$$\vec{p} = \tfrac{1}{2}(\vec{p}_2 - \vec{p}_3), \quad \vec{q} = \tfrac{2}{3}\big(\vec{p}_1 - \tfrac{1}{2}(\vec{p}_2 + \vec{p}_3)\big). \tag{4.2}$$

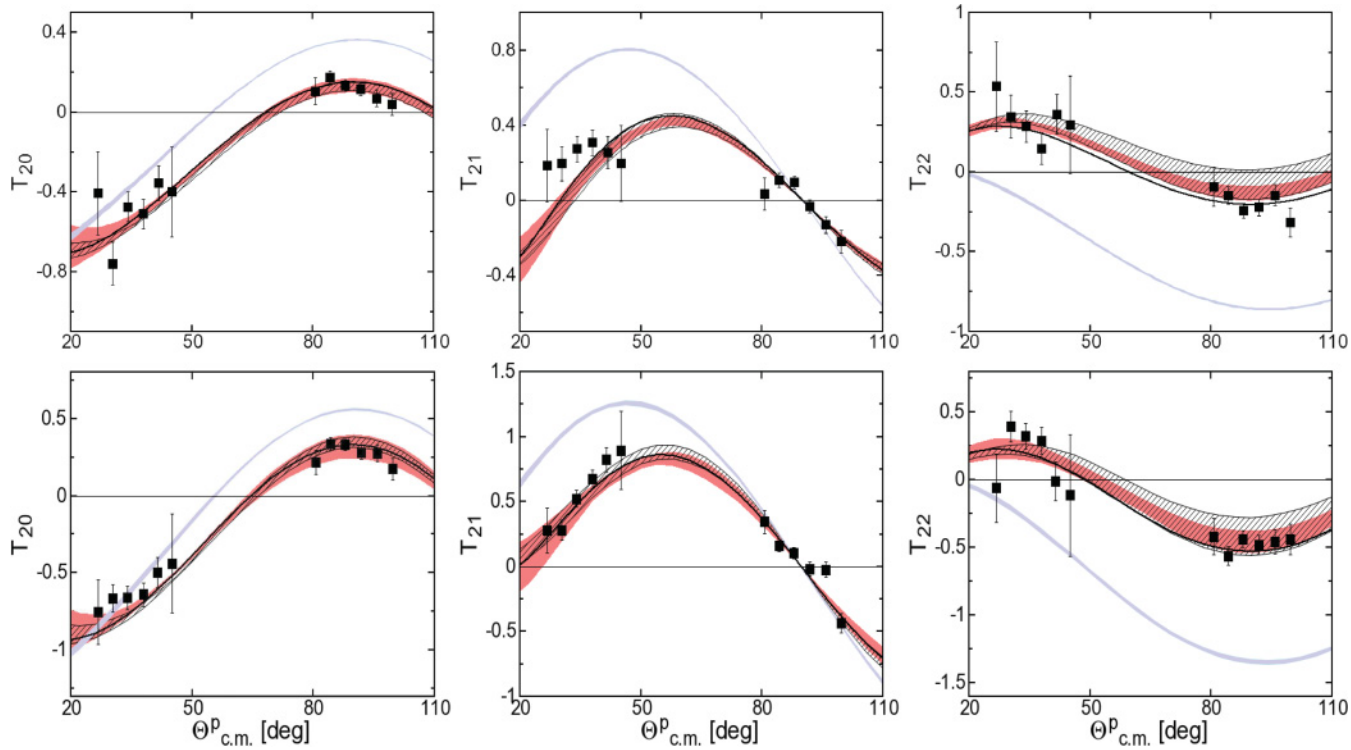

FIG. 2. (Color online) Deuteron tensor analyzing powers vs. proton emission angle for two E_γ energy bins. The upper row shows results for bin energy $E_\gamma = 25$–45 MeV. The lower row shows results for bin energy $E_\gamma = 45$–70 MeV. The bands and lines have the same meaning as in Fig. 1. The experimental data are from Rachek *et al.* [25].

We consider two types of $3N$ scattering states. In the first case two nucleons bound in the deuteron emerge with the accompanying third nucleon and the asymptotic motion of this unbound nucleon is described by the Jacobi momentum $\vec{q}_0$. In the second case, we have three free nucleons in the final state and their asymptotic relative motions are represented by $\vec{p}$ and $\vec{q}$.

To calculate the crucial matrix elements N^μ given in Eq. (4.1), it is not necessary to solve the corresponding Faddeev equations directly for the $3N$ scattering states [11]. Instead, we solve a Faddeev-type equation for an auxiliary state $|U\rangle$. In our calculations, we do not include the effects of $3N$ forces. Thus, the equation for $|U\rangle$ takes a simpler form

$$|U\rangle = tG_0(1+P)J^\mu(\vec{Q})\left|\Psi^{3N}_{\rm bound}\right\rangle + tG_0P\,|U\rangle. \quad (4.3)$$

The corresponding nuclear matrix elements are then given by

$$N^\mu_{Nd} = \langle\Phi_d|\,(1+P)J^\mu(\vec{Q})\left|\Psi^{3N}_{\rm bound}\right\rangle + \langle\Phi_d|\,P\,|U\rangle,$$
$$N^\mu_{Npn} = \langle\Phi_0|\,(1+P)J^\mu(\vec{Q})\left|\Psi^{3N}_{\rm bound}\right\rangle + \langle\Phi_0|\,(1+P)\,|U\rangle, \quad (4.4)$$

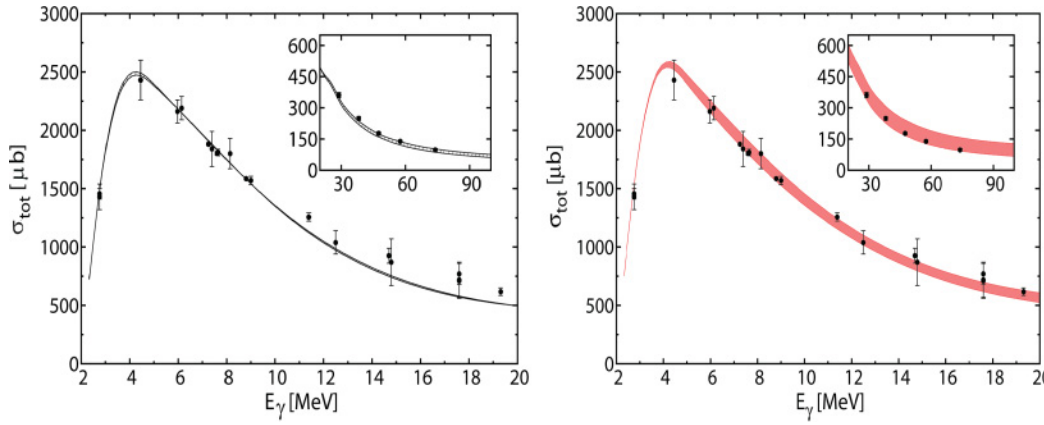

FIG. 3. (Color online) Total cross section for photodisintegration of the deuteron as a function of photon energy beam. In the left panel results for the single nucleon current and OPE contribution are shown. In the right panel, the results obtained with an additional TPE currents are given. The experimental data are the same as in Ref. [7].

with the NN t matrix in the $3N$ space, G_0 the free $3N$ propagator and P the permutation operator $P = P_{12}P_{23} + P_{13}P_{23}$. Further, $|\Phi_d\rangle$ is the antisymmetrized product state containing the deuteron and the momentum state for the relative motion of the third nucleon. Finally, $|\Phi_0\rangle$ is the antisymmetrized product state describing the two relative motions among the three outgoing nucleons. For details about the solution of Eqs. (4.3) and (4.4) see Ref. [11]. It is important to mention that these equations are solved in the partial wave basis. In the following, we therefore briefly discuss the partial wave decomposition of the current operator, which can generally be written in the form

$$J^\mu = J^\mu(1) + J^\mu(2) + J^\mu(3) + J^\mu(2,3) + J^\mu(3,1) + J^\mu(1,2). \tag{4.5}$$

There are three pairs in the $3N$ system, but it is sufficient to include a contribution just from one pair exploiting the fully antisymmetric nature of the $3N$ states. The two-nucleon current operator $J^\mu(2,3)$ is defined according to Eq. (2.5). Compared to Eq. (2.8), in the case of the $3N$ system, we have additional contributions from the T_1 isospin structure. Thus,the nonvanishing contributions emerge from

$$\vec{J}_{2\pi}(2,3) = \sum_{\beta=3}^{10} f_1^\beta(\vec{q}_2,\vec{q}_3) T_1 \vec{O}_\beta + \sum_{\beta=3}^{10} f_2^\beta(\vec{q}_2,\vec{q}_3) T_2 \vec{O}_\beta + f_3^2(\vec{q}_2,\vec{q}_3) T_3 \vec{O}_2, \tag{4.6}$$

where $\vec{q}_2$ and $\vec{q}_3$ are the momentum transfers of nucleons 2 and 3, respectively. We utilize the so-called jI coupling scheme for the $3N$ basis states

$$\begin{aligned} |p\,q\,\alpha\rangle &= \left|p\,q\,(ls)j\left(\lambda\tfrac{1}{2}\right)I\,(jI)\,JM\right\rangle\left|\left(t\tfrac{1}{2}\right)T\,M_T\right\rangle \\ &\equiv |p\,q\,\alpha_J\rangle|\alpha_T\rangle. \end{aligned} \tag{4.7}$$

Here, l, s, j, and t refer to the orbital angular momentum, spin, total angular momentum, and isospin of the (2–3) subsystem, respectively. The angular momentum of nucleon 1 is coupled with its spin $1/2$ to the total angular momentum I. Finally, the subsystem total angular momentum j is coupled with I to give the total $3N$ angular momentum J with the projection M. A similar coupling in the isospin space leads to the total $3N$ isospin T with the corresponding magnetic quantum number M_T.

Analogously to the procedure described in Sec. II, we compute the general matrix element of the $2N$ current in the $3N$ basis

$$\begin{aligned} \langle p'q'\alpha'|\vec{J}_{2\pi}(2,3)|pq\alpha\rangle &= \langle p'q'\alpha_{J'}|\vec{O}_\beta\, f_\eta^\beta(\vec{q}_2,\vec{q}_3)|pq\alpha_J\rangle\,\langle\alpha_{T'}|T_\eta|\alpha_T\rangle \\ &= \sum_{m_j,m_{j'}} C(j'I'J';m_{j'},M'-m_{j'},M')\,C(jIJ;m_j,M-m_j,M) I_{23}(p',p,Q;(l's')j'm_{j'},(ls)jm_j) \\ &\quad\times I_1\left[q',q,Q;\left(\lambda'\frac{1}{2}\right)I'M'-m_{j'},\left(\lambda\frac{1}{2}\right)IM-m_j\right]\langle\alpha_{T'}|T_\eta|\alpha_T\rangle, \end{aligned} \tag{4.8}$$

with

$$\begin{aligned} I_{23}(p',p,Q;(l's')j'm_{j'},(ls)jm_j) &= \int d\hat{p}' \int d\hat{p} \sum_{m_{l'}}\sum_{m_l} C(l's'j';m_{l'},m_{j'}-m_{l'},m_{j'}) Y^*_{l',m_{l'}}(\hat{p}') \\ &\quad\times C(lsj;m_l,m_j-m_l,m_j) Y_{l,m_l}(\hat{p})\, f_\eta^\beta(\vec{q}_2,\vec{q}_3)\,\langle s'\,m_{j'}-m_{l'}|\vec{O}_\beta|s\,m_j-m_l\rangle, \end{aligned} \tag{4.9}$$

and

$$I_1\left[q',q,Q;\left(\lambda'\frac{1}{2}\right)I'M'-m_{j'},\left(\lambda\frac{1}{2}\right)IM-m_j\right] = \int d\hat{q}'\,\mathcal{Y}^{I',M'-m_{j'}*}_{\lambda'\frac{1}{2}}(\hat{q}')\frac{\delta\left(q-\left|\vec{q}'+\frac{1}{3}\vec{Q}\right|\right)}{q^2}\mathcal{Y}^{I,M-m_j}_{\lambda\frac{1}{2}}\left(\widehat{\vec{q}'+\frac{1}{3}\vec{Q}}\right), \tag{4.10}$$

where we have introduced

$$\mathcal{Y}^{I\,\nu}_{\lambda\frac{1}{2}}(\hat{q}) \equiv \sum_m C\left(\lambda\frac{1}{2}I;m,\nu-m,\nu\right) Y_{\lambda,m}(\hat{q})\left|\frac{1}{2}\,\nu-m\right\rangle. \tag{4.11}$$

For I_{23}, we recognize the same type of a matrix element we dealt with in the $2N$ space. Now, however, the isospin part is separated out. This is because there are much more isospin combinations in the $3N$ system compared to processes on the deuteron that have the total isospin zero. This separation allows us, in particular, to calculate I_{23} once and use it both for the reaction on ^{3}He and ^{3}H. For the numerical implementation it is, however, still important to use the properties of the matrix elements $\langle\alpha_{T'}|T_\eta|\alpha_T\rangle$ $(\eta = 1,2,3)$ to reduce the number

of necessary four-fold integrals in I_{23}, even if the isospin dependence is now treated separately. Below we give the matrix elements of the three isospin operators in the $3N$ isospin space. As already mentioned, we assume that the operators act on the $3N$ bound state (^{3}He or ^{3}H), which has the total isospin $T = 1/2$. It is then straightforward to obtain

$$\left\langle \left(t'\frac{1}{2}\right) T' m_{T'} \middle| T_1 \middle| \left(t\frac{1}{2}\right)\frac{1}{2} m_T \right\rangle \equiv \left\langle \left(t'\frac{1}{2}\right) T' m_{T'} \middle| (\vec{\tau}(2)+\vec{\tau}(3))_3 \middle| \left(t\frac{1}{2}\right)\frac{1}{2} m_T \right\rangle$$
$$= C\left(1, \frac{1}{2}, T'; 0, m_T, m_{T'}\right) \sqrt{12}\sqrt{(2t'+1)(2t+1)} \begin{Bmatrix} 1 & t & t' \\ \frac{1}{2} & T' & \frac{1}{2} \end{Bmatrix} \begin{Bmatrix} 1 & \frac{1}{2} & \frac{1}{2} \\ \frac{1}{2} & t' & t \end{Bmatrix}$$
$$\times (-1)^{t+t'+\frac{1}{2}+T'} \left[1+(-1)^{t+t'}\right], \tag{4.12}$$

$$\left\langle \left(t'\frac{1}{2}\right) T' m_{T'} \middle| T_2 \middle| \left(t\frac{1}{2}\right)\frac{1}{2} m_T \right\rangle \equiv \left\langle \left(t'\frac{1}{2}\right) T' m_{T'} \middle| (\vec{\tau}(2)-\vec{\tau}(3))_3 \middle| \left(t\frac{1}{2}\right)\frac{1}{2} m_T \right\rangle$$
$$= C\left(1, \frac{1}{2}, T'; 0, m_T, m_{T'}\right) \sqrt{12}\sqrt{(2t'+1)(2t+1)} \begin{Bmatrix} 1 & t & t' \\ \frac{1}{2} & T' & \frac{1}{2} \end{Bmatrix} \begin{Bmatrix} 1 & \frac{1}{2} & \frac{1}{2} \\ \frac{1}{2} & t' & t \end{Bmatrix}$$
$$\times (-1)^{t+t'+\frac{1}{2}+T'} \left[1-(-1)^{t+t'}\right], \tag{4.13}$$

$$\left\langle \left(t'\frac{1}{2}\right) T' m_{T'} \middle| iT_3 \middle| \left(t\frac{1}{2}\right)\frac{1}{2} m_T \right\rangle \equiv \left\langle \left(t'\frac{1}{2}\right) T' m_{T'} \middle| i\,(\vec{\tau}(2)\times\vec{\tau}(3))_3 \middle| \left(t\frac{1}{2}\right)\frac{1}{2} m_T \right\rangle$$
$$= C\left(1, \frac{1}{2}, T'; 0, m_T, m_{T'}\right) 12\sqrt{3}\sqrt{(2t'+1)(2t+1)} \begin{Bmatrix} 1 & t & t' \\ \frac{1}{2} & T' & \frac{1}{2} \end{Bmatrix} \begin{Bmatrix} 1 & 1 & 1 \\ \frac{1}{2} & \frac{1}{2} & t \\ \frac{1}{2} & \frac{1}{2} & t' \end{Bmatrix}$$
$$\times (-1)^{1+t+\frac{1}{2}+T'}. \tag{4.14}$$

V. RESULTS FOR PHOTODISINTEGRATION OF ^{3}HE

We are now in the position to discuss our results for two- and three-body photodisintegration of ^{3}He at three example photon laboratory energies $E_\gamma = 12$, 20.5, and 50 MeV. The Coulomb force between two-protons in three-nucleon scattering states is not taken into account. The three-nucleon matrix elements $\vec{N}$ are obtained using the partial wave decomposition, with the total angular momentum of the three-nucleon system

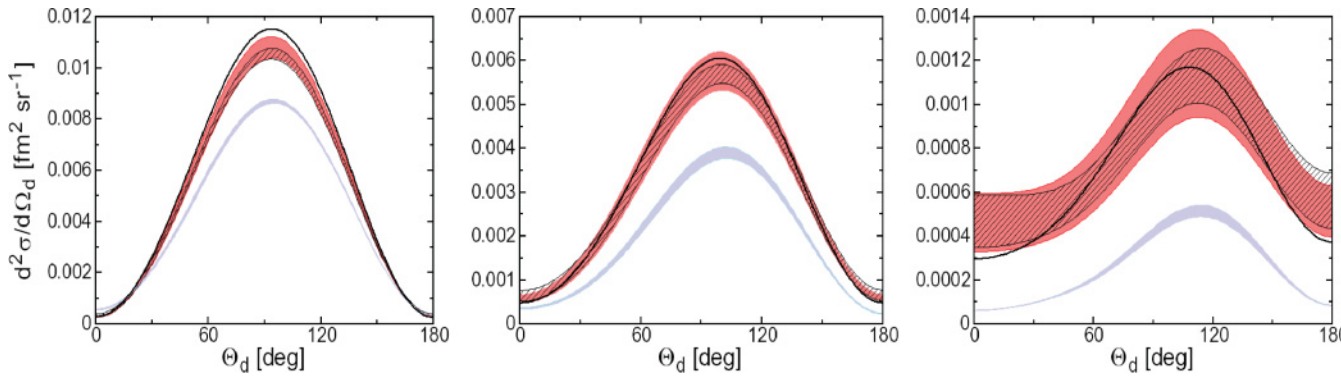

FIG. 4. (Color online) Differential cross section in the laboratory frame for ^{3}He two-body photodisintegration at the photon laboratory energies $E_\gamma = 12$ MeV (left), $E_\gamma = 20.5$ MeV (middle), and $E_\gamma = 50$ MeV (right). The band covers N^{2}LO chiral predictions for different cutoff parameter values. The light (blue) band covers results obtained with the single-nucleon current. In the case of the hatched band, the current operator is taken as a sum of the single nucleons current and OPE current. The dark (pink) band covers N^{2}LO chiral predictions for different cutoff parameter values and the current operator is taken as a sum of the single nucleons current, OPE current, and TPE current. The solid line represents predictions obtained with the AV18 nucleon-nucleon potential and the related exchange currents [11].

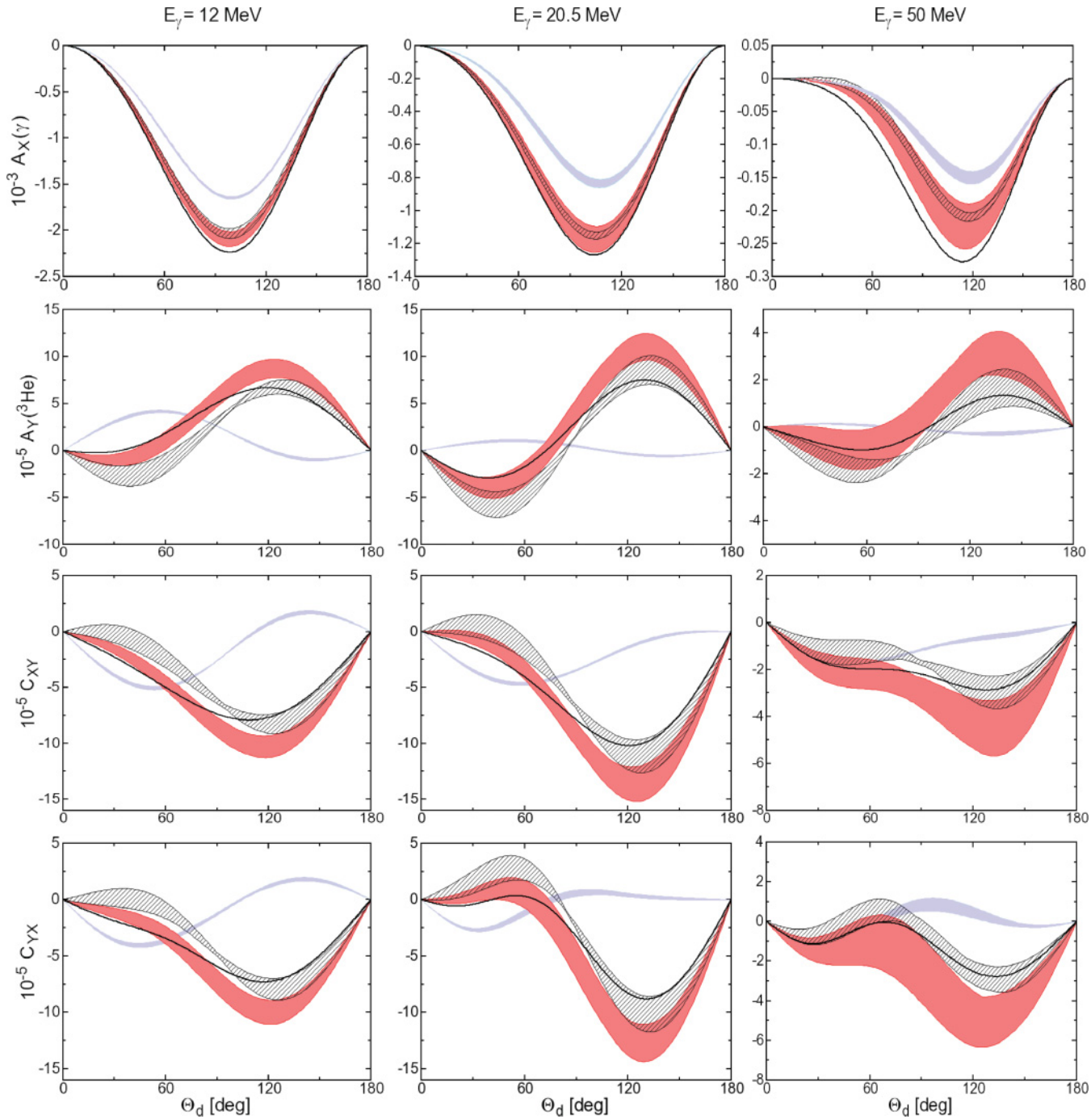

FIG. 5. (Color online) Spin observables for ^{3}He two-body photodisintegration at photon laboratory energy $E_\gamma = 12$ MeV (left), $E_\gamma = 20.5$ MeV (middle), and $E_\gamma = 50$ MeV (right). The upper rows show the analyzing powers for photon $[A_x(\gamma)]$ and ^{3}He $[A_y(^3\mathrm{He})]$. The lower rows show spin correlation coefficients C_{XY} and C_{YX}. The bands and lines have the same meaning as in Fig. 4.

$J \leqslant 15/2$ and including all partial waves with the subsystem total angular momentum $j \leqslant 3$. The nuclear matrix elements $\vec{N}$ are computed as using the formalism described in Sec. IV. Given $\vec{N}$, one can calculate cross sections and polarization observables that are expressed in terms of the nuclear matrix elements with different spin projections carried by the initial photon, the ^{3}He nucleus, and the outgoing nucleons and/or deuteron. For more details we refer the reader to Refs. [5,11]. In the following we just present our sample results for the ChEFT approach.

We begin with the exclusive unpolarized cross section for the two-body breakup of ^{3}He, $d^2\sigma/d\Omega_d$, where the final deuteron would be observed. It is depicted in Fig. 4 as a function of the deuteron scattering angle θ_d defined with respect to the initial photon direction at the photon laboratory energies $E_\gamma = 12$, 20.5, and 50 MeV. We observe a similar

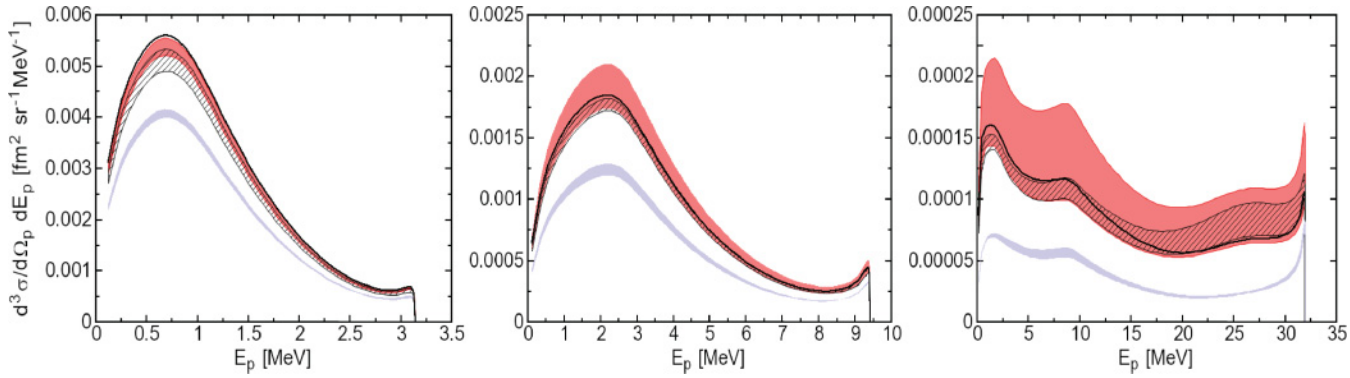

FIG. 6. (Color online) Differential cross section for semiexclusive ^{3}He three-body photodisintegration ^{3}He$(\gamma, p)pn$ for proton emissions at $\theta = 15^\circ$ and photon laboratory energy $E_\gamma = 12$ MeV (left), $E_\gamma = 20.5$ MeV (middle), and $E_\gamma = 50$ MeV (right). The bands and lines have the same meaning as in Fig. 4.

behavior as compared to the differential cross section in photodisintegration of the deuteron. The single nucleon current contribution yields significantly lower values as compared to the ones which include MECs. The TPE bands overlap with the OPE bands and appear to be broader than the OPE bands. As expected, the bands become wider with increasing photon energy.

Next, the results for a few polarization observables are shown in Fig. 5. We consider the photon $[A_x^\gamma(\theta_d)]$ and the ^{3}He $[A_y^{^3\mathrm{He}}(\theta_d)]$ analyzing powers as well as the spin correlation coefficients $C_{x,y}^{\gamma,^3\mathrm{He}}(\theta_d)$ and $C_{y,x}^{\gamma,^3\mathrm{He}}(\theta_d)$. In the case of the photon analyzing power $A_x(\gamma)$, the prediction bands for the single nucleon current give higher values than the other, more complete calculations, but the shape of the bands is always similar. The TPE bands are broader than the OPE bands and overlap with them. For the ^{3}He analyzing power $A_y(^3\mathrm{He})$ and the spin correlation coefficients C_{XY} and C_{YX}, we observe that the results based on ChEFT generate very broad prediction bands, especially at the highest energy considered. Interestingly, the results based on the single-nucleon current for these observables are completely different from the ones involving the MEC. This suggests that these observables are very sensitive to the details of the MECs, and their proper description will require the inclusion of the subleading OPE and short-range contributions not considered in the present work. We further emphasize that the results based on the AV18 potential and the corresponding MEC agree with the (present) ChEFT calculation.

For the three-body breakup of ^{3}He, we only show the semiexclusive differential cross section $d^3\sigma/d\Omega_p dE_p$ (where only one proton would be detected at 15 degrees with respect to the photon beam) at three photon laboratory energies $E_\gamma = 12$, 20.5, and 50 MeV. The calculated cross section is shown as a function of the proton energies in Fig. 6. For the lower photon energy (left panel), the obtained bands appear to be relatively narrow, especially for higher proton energies, where they both coincide with the AV18 results. For the lower proton energy the bands become broader. The TPE contributions bring the results close to the one obtained within the conventional framework. The situation is quite different for the highest photon energy (right panel). The shape of the calculated cross section is much more complicated in this case. Further, the band resulting from the TPE parts of the current operator appears to be very broad in the whole range of the proton energies. It remains to be seen whether the inclusion of the missing MEC contributions will allow to reduce the theoretical uncertainty for the cross section.

VI. CONCLUSION

In this work we explored the effects of the TPE currents derived recently in the framework of ChEFT [16] in the deuteron and ^{3}He photodisintegration reactions. We studied the role of various ingredients of the chiral $2N$ current operator in the unpolarized cross section and several polarization observables. As a main outcome of our study, we found that the new terms in the exchange current operator beyond the well-known OPE contribution play an important role for nearly all considered reactions. In particular, the differential cross section and the photon analyzing power in the deuteron photodisintegration process and the spin observables in ^{3}He two-body photodisintegration are found to provide an excellent testing ground for probing the fine details of the exchange current operator.

We also found that the inclusion of the TPE contribution to the current operator alone typically results in very broad bands for the considered observables. This behavior is not unexpected. The OPE and TPE MEC are computed in the framework of ChEFT within the low-momentum expansion and thus feature singular behavior at short distances (or large momenta). This leads to the observed large sensitivity of the calculated nuclear matrix elements to the short-distance behavior of the corresponding wave functions, which is strongly scheme and cutoff dependent. In a *complete* calculation, the cutoff dependence of the low-energy observables is expected to be strongly reduced by the "running" of the corresponding short-range current operators [see, e.g., Ref. [27] for the explicit examples of such a behavior in the case of the M1 properties of light nuclei within the hybrid approach and Ref. [28] for an extensive discussion on the (meaning of)

renormalization in the context of nuclear EFT with a finite cutoff]. Thus, the strong cutoff dependence in the obtained incomplete results that do not include the short-range contributions to the current operator should not be surprising. We expect that a complete NLO calculation including the short-range contact and the subleading OPE contributions to the $2N$ current operator will yield much narrower bands allowing for a quantitative description of electromagnetic reactions in a wider kinematical range. Work along these lines is in progress.

ACKNOWLEDGMENTS

This work was supported, in part, by the Polish Ministry of Science and Higher Education (Grant Nos. N N202 104536 and N N202 077435), the Helmholtz Association (Contract No. VH-NG-222), and the European Research Council (ERC-2010-StG 259218 NuclearEFT). The numerical calculations have been performed on the supercomputer cluster of the JSC, Jülich, Germany.

[1] T. S. Park, D.-P. Min, and M. Rho, Phys. Rept. **233**, 341 (1993).
[2] T. S. Park, K. Kubodera, D. P. Min, and M. Rho, Phys. Lett. B **472**, 232 (2000).
[3] M. Walzl and U.-G. Meißner, Phys. Lett. B **513**, 37 (2001).
[4] D. Phillips, in *Proceedings of the 6th International Workshop on Chiral Dynamics*, PoS **(CD09) 066** (2009).
[5] R. Skibinski, J. Golak, H. Witała, W. Gloeckle, A. Nogga, and E. Epelbaum, Acta Phys. Polon. B **37**, 2905 (2006).
[6] D. Shukla, A. Nogga, and D. R. Phillips, Nucl. Phys. A **819**, 98 (2009).
[7] H. Arenhövel and M. Sanzone, Few-Body Syst. Suppl. **3**, 1 (1991).
[8] R. Gilman and F. Gross, J. Phys. G: Nucl. Part. Phys. **28**, R37 (2002).
[9] J. Carlson and R. Schiavilla, Rev. Mod. Phys. **70**, 743 (1998).
[10] L. E. Marcucci, A. Kievsky, L. Girlanda, S. Rosati, and M. Viviani, Phys. Rev. C **80**, 034003 (2009).
[11] J. Golak *et al.*, Phys. Rep. **415**, 89 (2005), and references therein.
[12] E. Epelbaum, Prog. Part. Nucl. Phys. **57**, 654 (2006).
[13] E. Epelbaum, H.-W. Hammer, and U.-G. Meißner, Rev. Mod. Phys. **81**, 1773 (2009).
[14] S. Pastore, R. Schiavilla, and J. L. Goity, Phys. Rev. C **78**, 064002 (2008).
[15] S. Pastore, L. Girlanda, R. Schiavilla, M. Viviani, and R. B. Wiringa, Phys. Rev. C **80**, 034004 (2009).
[16] S. Kölling, E. Epelbaum, H. Krebs, and U.-G. Meißner, Phys. Rev. C **80**, 045502 (2009).
[17] V. V. Kotlyar, Few-Body Syst. **28**, 35 (2000).
[18] L. L. Foldy and J. A. Lock, in *Mesons In Nuclei*, edited by M. Rho and D. Wilkinson, Vol. II. (North-Holland, Amsterdam, 1979).
[19] W. Glöckle, *The Quantum Mechanical Few-Body Problem* (Springer-Verlag, Berlin/Heidelberg, 1983).
[20] J. Golak *et al.*, Eur. Phys. J. A **43**, 241 (2010).
[21] R. B. Wiringa, V. G. J. Stoks, and R. Schiavilla, Phys. Rev. C **51**, 38 (1995).
[22] D. O. Riska, Phys. Scr. **31**, 107 (1985).
[23] D. O. Riska, Phys. Scr. **31**, 471 (1985).
[24] S. Ying, E. M. Henley, and G. A. Miller, Phys. Rev. C **38**, 1584 (1988).
[25] I. A. Rachek *et al.*, Phys. Rev. Lett. **98**, 182303 (2007).
[26] A. Nogga, A. Kievsky, H. Kamada, W. Glöckle, L. E. Marcucci, S. Rosati, and M. Viviani, Phys. Rev. C **67**, 034004 (2003).
[27] Y.-H. Song, R. Lazauskas, T.-S. Park, and D.-P. Min, Phys. Lett. B **656**, 174 (2007).
[28] G. P. Lepage, arXiv:nucl-th/9706029.